Further Study on Strain Growth in Spherical Containment Vessels Subjected to Internal Blast Loading

Q. Dong, Q.M. Li, J.Y. Zheng

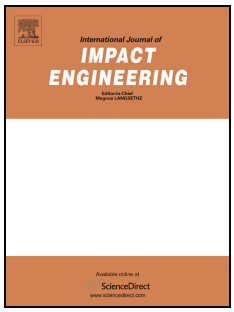

Title: Further Study on Strain Growth in Spherical Containment Vessels Subjected to Internal Blast Loading

Authors: Q. Dong, Q.M. Li, J.Y. Zheng

PII: S0734-743X(09)00163-8

DOI: 10.1016/j.ijimpeng.2009.09.001

Reference: IE 1830

To appear in: *International Journal of Impact Engineering*

Received Date: 26 August 2008

Revised Date: 30 August 2009

Accepted Date: 2 September 2009

Please cite this article as: Dong Q, Li QM, Zheng JY. Further Study on Strain Growth in Spherical Containment Vessels Subjected to Internal Blast Loading, International Journal of Impact Engineering (2009), doi: 10.1016/j.ijimpeng.2009.09.001

Further Study on Strain Growth in Spherical Containment Vessels Subjected to Internal Blast Loading

Q.Dong[1], Q.M.Li[2*], J.Y.Zheng[3]

[1]Institute of Fluid Physics, China Academy of Engineering Physics, Mianyang 621900, P. R. China

[2]School of Mechanical, Aerospace and Civil Engineering, Pariser Building

The University of Manchester, PO Box 88, Manchester M60 1QD, UK

[3]Institute of Process Equipment, Zhejiang University, Hangzhou 310027, P.R.China

Abstract: Strain growth is a phenomenon observed in the elastic response of containment vessels subjected to internal blast loading, which is featured by the increased vibration amplitude of the vessel in a later stage. Previous studies attributed the strain growth in spherical containment vessels to the beating between two close vibration modes, the interactions between the vessel vibration and the reflected shock waves and the structural perturbation. In this paper, it is shown that nonlinear modal coupling is another important cause of strain growth in spherical containment vessels. Based on the understanding of the vibration modes in a complete spherical shell, the nonlinear modal coupling in the nonaxisymmetric response of complete spherical shells are studied using finite element method. Methods for preventing the strain growth due to nonlinear modal coupling are discussed, which provide guidelines for the engineering design of spherical containment vessels.

Keywords: strain growth, containment vessel, spherical shell, nonaxisymmetic vibration modes, nonlinear modal coupling

* Corresponding author, e-mail: qingming.li@manchester.ac.uk; Fax: +44(0)1613063849

1. Introduction

Containment vessels have been widely used to contain the blast effects in civil, military and industrial applications (Zheng et al. 2006). One unresolved problem in the design of multiple-use containment vessels is the strain growth phenomenon (Nickell and Romero 2003).

Strain growth is a phenomenon observed in the elastic response of containment vessels subjected to internal blast loading. The dynamic response of a containment vessel during the initial stage can be described by the radial breathing mode (RBM). However, transformation from RBM to flexural mode may occur in a later stage, leading to increased local deformation, and possibly unexpected local plastic deformation and accelerated fatigue failure, in containment vessels designed for multiple-use purpose. Therefore, it is necessary to understand the mechanisms of strain growth in containment vessels.

Strain growth phenomenon was observed in 1976 (Buzukov 1976). Since then, the mechanisms of strain growth in spherical and cylindrical containment vessels have been widely investigated. As the reflected shock waves after the first peak of the blast shock wave may still be strong, strain growth was once attributed to the possible resonance between the reflected shock waves and the vibration of the vessel [i.e. (Buzukov 1980) for cylindrical shells and (Zhdan 1981) for spherical shells]. Karpp et al.(1983) and Abakumov et al.(1984) showed that bending responses could be excited by the structural perturbation and the added mass associated with the structural pertubation (e.g. flanges), which could introduce localised deformations. Other researchers proposed that the superposition (or beating) of various vibration modes with close frequencies is responsible for strain growth in cylindrical (Buzukov 1976, Kornev et al. 1979, Zhu et al. 1997) and spherical (Mal'tsev et al. 1984, Belov et al. 1984, Duffey and Romero 2003) containment vessels. Detailed investigations on the strain growth phenomenon have been summarized in Duffey and Romero(2003) and Li et al.(2008). In summary, three mechanisms have been so far proposed to explain the strain growth phenomenon in spherical containment vessels, i.e. (i) resonance caused by reflected shock waves, (ii) the influence of structural perturbation, and (iii) superposition (or beating) of various vibration modes with close frequencies.

The recongnization of the above strain growth mechanisms are based on the linear responses of spherical containment vessels without considering the nonlinear modal coupling response. Li et al.(2008) and Dong et al.(2008) recently showed that the nonlinear modal coupling between the breathing mode and bending modes, which are excited by the dynamic unstable vibration, may also lead to strain growth in cylindrical containment vessels. The nonlinear modal coupling in spherical shells was studied by McIvor and Sonstegard(1966) and Nayfeh and Arafat(2006), which, however, concerned only the axisymmetric response of spherical shells. With the consideration of structural pertubations and the erratic response [i.e. due to the non-uniform blast loading (Baker 1960)] in

spherical containment vessels, the responses of a spherical containment vessel are generally nonaxisymmetric. Therefore, in order to fully understand the responses of spherical containment vessels, the nonlinear modal coupling in the nonaxisymmetric responses of spherical containment vessels subjected to internal blast loading should be investigated.

The axisymmetric and nonaxisymmetric vibrational modes of spherical shells with and without imperfections, and the nonlinear vibrations of axisymmetric spherical shells are presented in Section 2. Finite element analysis on the full 3-D shell model is employed in Section 3 to study the nonlinear modal coupling in the nonaxisymmetric response of spherical shells subjected to internal impulsive loading. Based on the understanding of the strain growth mechanism due to nonlinear modal coupling, methods for preventing the strain growth in spherical containment vesssels are discussed in Section 3, which is followed by conclusions in Section 4.

2. Vibrations of complete spherical shells

Strain growth in a spherical containment vessel is closely related to the axisymmetric and nonaxisymmetric vibrational modes and the nonlinear vibration of the spherical shell, which will be introduced briefly in this section.

2.1 Axisymmetric vibration of a spherical shell

In a complete spherical shell, the axisymmetric modes are independent of the circumferential coordinate. Previous works have been reported in Baker(1961), Kalnins(1964) and Wilkinson(1965) and reviewed by Duffey and Romero(2003). When the shear and torsional responses are neglected, the axisymmetric vibration of a complete spherical shell has following non-dimensional frequencies ω_n (McIvor and Sonstegard 1966, Nayfeh and Arafat 2006)

$$\omega_0 = [2(1+\nu)]^{1/2}, \tag{1a}$$

$$\begin{aligned} 2\omega_n^{\ 2} = {} & 1+3\nu-\alpha^2(1-\nu)+n(n+1)(1+\nu\alpha^2)+\alpha^2 n^2(n+1)^2 \pm [9+6\nu+\nu^2 \\ & +2\alpha^2(3+\nu)(1-\nu)+2n(n+1)(2\nu^2+3\nu-1)+n^2(n+1)^2 \\ & +2\alpha^2 n(n+1)(5\nu^2+2\nu-11)+2\alpha^2 n^2(n+1)^2(9+4\nu)-2\alpha^2 n^3(n+1)^3 \\ & -2\alpha^4 n(n+1)\nu(1-\nu)+\alpha^4 n^2(n+1)^2(\nu^2+2\nu-2) \\ & +2\nu\alpha^4 n^3(n+1)^3+\alpha^4 n^4(n+1)^4]^{1/2}. \end{aligned} \tag{1b}$$

where ν is Possion's ratio; $\alpha = h/\sqrt{12}a$, in which h is the thickness and a is the radius of the spherical shell; n is the mode number.

Equation (1b) has two branches of expressions for $\omega_n^{\ 2}$, i.e., $(\omega_n^m)^2$ for the positive sign (i.e. upper branch) and $(\omega_n^c)^2$ for the negative sign (i.e. lower branch). When n=0, the mode of

vibration is a centrally symmetric radial motion i.e. the radial breathing mode (RBM). For each value of $n \geq 1$, there are two modes corresponding to the natural frequencies ω_n^m and ω_n^c, respectively. It was observed that the frequencies ω_n^m are relatively independent of *a*/*h*, whereas the frequencies ω_n^c are sensitive to the changes of *a*/*h* (McIvor and Sonstegard 1966, Nayfeh and Arafat 2006). McIvor and Sonstegard(1966) found that the vibration modes associated with ω_n^m are membrane modes whereas the ω_n^c modes changes from membrane-dominated modes to bending-dominated modes as *n* increases. Therefore, the modes associated with frequencies ω_n^m and ω_n^c are classified as membrane and composite modes, respectively. Duffey and Romero(2003) and Duffey et al.(2007) confirmed the existence of two branches of modes in the axisymmetric vibration of spherical shells using finite element analysis and experimental investigation.

According to the relationship between the natural frequency f and the non-dimensional frequency ω i.e. $f = \omega\{E/[(1-\nu^2)\rho]\}^{1/2}/(2\pi a)$, in which E is Young's modulus and ρ is the density, the natural frequency of the radial breathing mode is

$$f_0 = \frac{1}{2\pi a}\sqrt{\frac{2E}{\rho(1-\nu)}}, \tag{2a}$$

and the natural frequency of the *n*th vibration mode is

$$f_n = \omega_n \frac{1}{2\pi a}\sqrt{\frac{E}{\rho(1-\nu^2)}}. \tag{2b}$$

2.2 Nonaxisymmetric vibration of complete spherical shells

In a complete spherical shell, the nonaxisymmetric modes depend upon both the circumferential and longitudinal coordinates. Silbiger(1960, 1965) first studied the nonaxisymmetric modes of spherical shells and proposed that nonaxisymmetric modes are degenerate i.e. their frequencies are identical to the corresponding frequencies of axisymmetric modes. Silbiger(1960, 1965) explained mathematically that the eigenfunctions corresponding to the modes of a spherical shell are degenerate and attributed this degeneracy to the spherical symmetry of the shell. Silbiger(1960, 1965) pointed out that the axisymmetric modes should be defined with respect to a selected axis of reference. However, if a different orientation of the axis is chosen, the shell can vibrate in the same modes due to the symmetry, which may be independent of the axisymmetric modes about other reference axes even though they have the same frequency. Silbiger(1960, 1965) showed that as a consequence of the spherical symmetry in spherical shells, the *n*th nonaxisymmetric modes can be obtained by superposing the *n*th axisymmetric modes with respect to different axes, in which the new nonaxisymmetric modes still have the same frequency as

the *n*th axisymmetric mode but are not symmetric with respect to any axis. For each integer $n>1$, there is one independent axisymmetric mode and $2n$ independent nonaxisymmetric modes, given by $m=0$ and $m=1, 2\ldots n$, respectively, corresponding to the wave numbers *m* along the circumferential equator (Silbiger 1960, 1965). More precisely, $2n+1$ linearly independent modes can be constructed from the *n*th axisymmetric mode in each branch. All other vibration modes, which have the same frequency of the *n*th axisymmetric mode, are the linear combinations of these $2n+1$ independent modes (Silbiger 1960, 1965). Shah et al.(1969) and Niordson(1984) also proposed that the nonaxisymmetric modes of a given degree *n* can be obtained by superposing a number of the *n*th axisymmetric modes about different axes, if proper axes and amplitudes are chosen, in which the frequencies of the *n*th nonaxisymmetric modes are the same as the *n*th axisymmetric mode.

Duffey and Romero(2003) and Duffey et al.(2007) performed finite element modal calculations to investigate the nonaxisymmetric vibration of spherical shells, including the effect of bending and shear. It was observed that for each value of *n* in each branch, there are $2n+1$ modes in the nonaxisymmetric vibration, which is exactly the number predicted by Silbiger(1965). Duffey and Romero(2003) and Duffey et al.(2007) showed that among the $2n+1$ modes for each *n* in each branch, one is the corresponding axisymmetric mode, and the other $2n$ modes are degenerate nonaxisymmetric modes. As an illustration of mode shapes, the axisymmetric and nonaxisymmetric modes for $n=5$ in the lower branch are presented in Fig.1 using an ALGOR finite element model (Duffey et al. 2007). It was also observed that the nonaxisymmetric modes occur in pairs, which differ only an angle of π/n rigid body rotation with respected to the vertical axis (Duffey et al. 2007).

2.3 Vibration of spherical shells with imperfections

According to Duffey and Romero(2003), a real spherical containment vessel can be treated as a perturbated complete spherical shell. For the vibration of spherical shells with imperfections, Silbiger(1965) predicted that a deviation from spherical symmetry can remove the degeneracy and therefore the frequencies of *n*th vibration modes in each branch will split into $2n+1$ distinct frequencies.

Niordson(1988) investigated the distribution of natural frequencies in an open thin elastic spherical shell and discovered that due to the asymmetry caused by the hole, the frequency spectrum displayed a band structure, which indicates the similar prediction as that proposed by Silbiger(1965). The relation between the asymmetry and bandwidth was observed, i.e. the smaller the asymmetry is, the narrower the band is. It was also found that the distinct frequencies in narrow bands are close to the frequencies of the corresponding complete spherical shell (Niordson 1988).

Duffey and Romero(2003) investigated the nonaxisymmetric vibration of a spherical containment vessel with nozzles, which can be regarded as an imperfect spherical shell. Even though the spherical symmetry is destroyed by the imperfection, the natural frequency of a spherical containment vessel calculated by ABAQUS is close to the frequency of the corresponding complete spherical shell (Duffey and Romero 2003), which agrees with the finding in Niordson(1988). According to the finite element calculations and experimental results in the vibration of imperfect spherical shells, Duffey and Romero(2003) and Duffey et al.(2007) demonstrated the splitting phenomenon predicted by Silbiger(1965) i.e. the *n*th vibration frequencies split into 2*n*+1 independent distinct frequencies due to the deviation from spherical symmetry.

2.4 Nonlinear vibration of axisymmetric spherical shells

McIvor and Sonstegard(1966) studied the dynamic nonlinear vibration in the axisymmetric response of a closed spherical shell subjected to a nearly uniform radial impulse. The response of the closed spherical shell is a pure radial motion, i.e. radial breathing mode vibration when the shell is subjected to a perfectly-uniform radial impulse. However, if the impulse is slightly nonuniform (or equivalently, the spherical shell has imperfections), the membrane radial breathing mode may be dynamically unstable due to the interaction between the membrane stress and the flexural curvature (McIvor and Sonstegard 1966). The nonlinear coupling between the radial breathing mode and composite modes may happen during the dynamic unstable vibration of the spherical shell. In addition, it was shown that a cyclic energy exchange may occur between the radial breathing mode and high-order composite modes. The Mathieu equation that controls the development of the *n*th composite mode is (McIvor and Sonstegard 1966)

$$d^2 b_n / d\bar{\tau}^2 + (\Omega_n - \mu_n \sin\bar{\tau}) b_n = 0, \quad n \geq 2, \tag{3}$$

where b_n a non-dimensional coefficient describing the amplitude of the *n*th composite mode, $\bar{\tau} = \omega_0 \tau$, in which τ is the non-dimensional time defined as $\tau = ct/a$ (t is the time) and the elastic wave speed $c = \sqrt{E/\rho(1-\nu^2)}$, and

$$\Omega_n = (\omega_n^c)^2 / \omega_0^{\ 2} = \{\omega_0^{\ 2}[1 + (\delta_n^b)^2 n(n+1)]\}^{-1}$$
$$\times \{2(1+\nu)[1+\delta_n^b n(n+1)] + n(n+1)[n(n+1)-1+\nu][(\delta_n^b)^2 + \alpha^2(1+\delta_n^b)^2]\}, \tag{4a}$$

$$\mu_n = (v_0 / c\omega_0^{\ 3})[1 + (\delta_n^b)^2 n(n+1)]^{-1}$$
$$\times \{[1-(\delta_n^b)^2] n(n+1)(1+\nu) + 2(\delta_n^b)^2 n(n+1)[n(n+1)-1+\nu] + 4\delta_n^b(1+\nu)n(n+1)\}. \tag{4b}$$

where v_0 is the initial radial velocity and the amplitude ratio δ_n^b in Eq.(4) is (McIvor and Sonstegard 1966)

$$\delta_n^b = \frac{1+\nu-\alpha^2(1-\nu)+\alpha^2 n(n+1)}{[1-\nu-n(n+1)](1+\alpha^2)+(\omega_n^c)^2}, \quad (5)$$

where the non-dimensional frequencies are given in Eq.(1). It is shown that if the point (Ω_n, μ_n) is in the unstable region of the Mathieu stability diagram, the nonlinear modal coupling in the axisymmetric response of spherical shells will happen.

Nayfeh and Arafat (2006) also showed that the internal resonances between the different types of modes may happen in the nonlinear vibration in the axisymmetric response of spherical shells.

3. Results and analysis

In this section, the mechanism and influential factors of the nonlinear modal coupling in the nonaxisymmetric response of spherical shells subjected to internal impulsive loading will be investigated in Sections 3.1 and 3.2, respectively, based on which the design considerations for the control of strain growth in spherical containment vesssels will be discussed in Section 3.3.

3.1 Dynamic nonaxisymmetric responses of spherical shells subjected to internal impulsive loading

In the present study, the dynamic responses of complete spherical shells subjected to internal impulsive loading will be studied using the finite element software LS-DYNA (Livermore Software Technology Corporation 1998, 2003). Since the response of the shell is elastic, isotropic lineal elastic model is used for the shell material.

3.1.1 Numerical model description

As shown in Section 2, nonaxisymmetric modes also exist in the elastic responses of a spherical shell. Therefore, all spherical shells will be modelled by three-dimensional full shells using solid elements. The shell is meshed into 6, 96 and 96 parts along the radial, circuferential and longitidunal directions, respectively, using Lagrangian method. Convergence tests have shown that the above mesh size can give reasonable results. Additionally, the time step used in all simulations will be 1 μs, which is small enough to capture the peak values.

In the present study, the internal blast loading is assumed to be an ideal, perfectly symmetric loading, without considering the erratic response (i.e. the nonuniform blast loading) after the second shock and the additional vibration modes excited by this non-uniformity (Baker 1960). It has been shown that if the effect of reflected shock waves is not considered, the simplification of the blast loading into an impulsive loading does not influence the occurrence of strain growth caused by nonlinear modal coupling (Li et al. 2008). Therefore, the internal blast loading is replaced by a uniformly-distributed internal impulsive loading with impulse (I), which can be related to an initial

radial velocity (v_0) by $v_0 = \frac{I}{\rho h}$. It will be shown later that the initial velocity can be represented by the first peak strain defined as the maximum strain (i.e. the ratio of the maximum radial displacement to the radius) in the first vibration period.

The material properties and structural dimensions of Shell 1, which is taken as the illustrative example in the present study, are listed in

Table 1.

3.1.2 Radial breathing mode response in a complete spherical shell

If a spherical shell is subjected to a centrally symmetric internal pressure pulse, the dynamic response of the shell is normally assumed to be centrally symmetric. Thus, the shell can be simplified into a single degree of freedom (SDoF) model with the radial displacement as the only degree of freedom. The SDoF response of the spherical shell is the so-called radial breathing mode vibration, which is controlled by (Baker 1960)

$$\frac{d^2w}{dt^2} + \beta_0^2 w = \frac{p(t)}{\rho h}, \tag{6}$$

where w is the radial displacement; $p(t)$ is the transient pressure pulse; β_0 is the circular frequency of the radial breathing mode given by $\beta_0 = 2\pi f_0$.

In this study, the complete spherical Shell 1 is subjected to an impulsive pressure pulse causing a first peak strain of 0.0005. Finite element simulation results demonstrate that the radial breathing mode response happens, as shown by the radial displacement-time history and the frequency spectrum in Fig.2(a,b), in which, f_0 represents the radial breathing mode frequency of the spherical shell. The radial breathing mode frequency shown in Fig.2(b) is 6.843 kHz, which is very close to the value 6.966 kHz according to the theoretical analysis using Eq.(2a). The deformed shape of Shell 1 shows that only the radial breathing mode shape is observed in the whole response period. However, the model of the radial breathing mode cannot predict the strain growth phenomenon.

3.1.3 Characteristics and mechanism of nonlinear modal coupling response

In order to understand the mechanism of the nonlinear modal coupling in the nonaxisymmetric responses of spherical shells, the vibration modes of Shell 1 are studied theoretically and numerically. According to Eq.(2), the natural frequencies of the membrane and composite modes in Shell 1 are calculated, as presented in Fig.3. The two branches in Fig.3 show similar characteristics to the results obtained by Duffey and Romero(2003). The upper and lower branches correspond to the membrane and composite modes, respectively. The natural frequencies of the axisymmetric and nonaxisymmetric vibration modes in Shell 1 are also calculated by ANSYS (ANSYS 2004), which agree well with the analytical results according to Eq.(2). The characteristics of the nonaxisymmetric vibration modes observed in ANSYS show good agreement with those described by Duffey and Romero(2003) and Duffey et al.(2007).

When the complete spherical Shell 1 is subjected to a higher impulsive loading, a late-time increase of the response caused by nonlinear modal coupling is observed in LS-DYNA simulation.

When the first peak strain is 0.005 in Shell 1, the radial, circumferential and latitudinal response histories are presented in Figs.4-6, respectively.

Figures 4-6 show that the response of Shell 1 in the earlier stage is a radial breathing mode vibration. However, after multiple cycles of vibration with the same vibration amplitude, the composite modes are excited, as demonstrated by the response histories in later stages in Figs.4(a), 5 and 6 and the frequency spectrum in Fig.4(b), in which f_c is the ferequency of the composite mode. The observed strain growth in the later stage is attributed to the nonlinear coupling between the breathing mode and the excited composite modes.

In the early stage, the deformed shape of Shell 1 is the radial breathing mode shape. However, in the late stage when strain growth happens, some nonaxisymmetric composite modes are excited, as shown in the deformed shapes in Fig.7 where the paired nonaxisymmetric composite modes n=m=12 are observed. In order to make the motion visible, the displacement has been multiplied by 10 in Fig.7.

According to Eq.(4) from McIvor and Sonstegard(1966) and the theory of Mathieu functions (McLachlan 1947), the dynamic axisymmetric response of a spherical shell may be unstable when (Ω_n, μ_n) is in the unstable region of the Mathieu stability diagram, especially when Ω_n is close to 1/4 or 1. It has been shown in Section 2 that the nonaxisymmetric modes of a given degree n can be obtained by superposing a number of axisymmetric modes of degree n (Silbiger 1960, 1965; Shah et al. 1969; Niordson 1984). We propose the following postulate, i.e.

Postulate-1: McIvor and Sonstegard(1966)'s analytical method for the nonlinear modal coupling between axisymmetric modes in a spherical shell is applicable to predict the occurrence of the nonlinear modal coupling between nonaxisymmetric modes in the same spherical shell.

Therefore, Eqs.(3-5) will be used in the following analyses for the nonaxisymmetric responses of spherical shells.

In the radial breathing mode response of a spherical shell, the maximum potential energy of the deformation is

$$U = \frac{1}{2}\int_{vol}(\sigma_\theta \varepsilon_\theta + \sigma_\phi \varepsilon_\phi)dV = \frac{E w_{\max}^{b\ 2}}{(1-\nu)a^2}V, \tag{7}$$

where V is the volume of the shell material, $\sigma_\theta = \sigma_\phi = \sigma$, $\varepsilon_\theta = \varepsilon_\phi = \varepsilon$, in which σ is the in-plane membrane stress, ε is the in-plane membrane strain, $w_{\max}^b$ is the maximum radial displacement in the radial breathing mode response, and θ and ϕ are circumferential and longitude coordinates. The maximum kinetic energy is

$$T = \frac{1}{2}\int_{vol} \rho(\frac{\partial r}{\partial t})^2 dV = \frac{\rho}{2} v_0^2 V \,, \tag{8}$$

in which $r = a + w$. Equating maximum values of the potential and kinetic energies and using $c = \sqrt{E/\rho(1-\nu^2)}$, we obtain

$$\frac{v_0}{c} = \frac{w_{\max}^b}{a}\sqrt{2(1+\nu)} \,. \tag{9}$$

According to Eq.(1a) i.e. $\omega_0 = [2(1+\nu)]^{1/2}$, the relationship between v_0 / c and first peak strain $\varepsilon_{\max}^b$ in the radial breathing mode response (i.e. $\varepsilon_{\max}^b = w_{\max}^b / a$) is

$$\frac{v_0}{c} = \varepsilon_{\max}^b \omega_0 \,. \tag{10}$$

According to the analytical method on the axisymmetric response of spherical shells in McIvor and Sonstegard(1966), Mathieu diagram of Shell 1 with a first peak strain 0.005 is drawn in Fig.8, which shows that some composite modes are unstable in the vibration. Therefore, strain growth and nonaxisymmetric composite modes in Shell 1 can be observed in the spherical shell when the first peak strain is 0.005. The nonlinear modal coupling between the radial breathing mode and composite modes can be considered as another cause of strain growth in spherical containment vessels.

3.2 Influential factors in nonlinear modal coupling response

According to the Mathieu equation obtained by McIvor and Sonstegard(1966), the first peak strain and the radius-to-thickness ratio are two dominant factors influencing the strain growth phenomenon in spherical shells. In this section, the effects of the first peak strain and the radius-to-thickness ratio on the determination of the occurrence and degree of strain growth will be studied.

3.2.1 Dimensional analysis

In this study, the strain growth time t_P is defined as the duration from the beginning to the moment when the maximum radial displacement appears, and the strain growth factor K_p is defined as the ratio of the maximum radial displacement in the whole vibration period to the first peak radial displacement.

It may be assumed that the strain growth time t_P depends on the material properties of the spherical shell, geometrical dimensions and the impulsive loading, represented by E, ρ, ν, h, a and $\varepsilon_{\max}^b$, in which the first peak strain $\varepsilon_{\max}^b$ can represent the impulsive loading. Therefore, $t_p = F_1\left(E, \rho, \nu, h, a, \varepsilon_{\max}^b\right)$. Relationship between t_p and the two affecting factors (i.e. the first peak

strain and the radius-to-thickness ratio) can be obtained by the dimensional analysis, which can be shown in a non-dimensional expression, i.e.

$$\frac{t_p}{a/\sqrt{\frac{E}{\rho}}} = F_2\left(\nu, \frac{h}{a}, \varepsilon_{\max}^b\right). \tag{11}$$

Equation (11) can be rewritten as

$$\frac{t_p}{T_0} = F_3\left(\nu, \frac{h}{a}, \varepsilon_{\max}^b\right), \tag{12}$$

in which the non-dimensional factor t_p/T_0, which is the ratio of the strain growth time t_p to the fundamental period T_0 of the radial breathing mode ($T_0=1/f_0$), is an approximate estimation of the oscillation numbers of the radial breathing mode vibration from the beginning to the moment when the maximum response in the strain growth stage appears.

Similarly, the relationship between K_p and the two influential factors (i.e. the first peak strain and the radius-to-thickness ratio) can be expressed as a function of three non-dimensional numbers, i.e.

$$K_p = F_4\left(\nu, \frac{h}{a}, \varepsilon_{\max}^b\right). \tag{13}$$

3.2.2 The first peak strain

The responses of Shell 1 under different first peak strains are calculated using LS-DYNA, as summarised in

Table 2, where the first peak strains of Shell 1 are 0.0040, 0.0045, 0.0050, 0.0055 and 0.006, respectively.

Relationships between t_p/T_0 and the first peak strain are drawn in Fig.9, which shows that strain growth time decreases as the first peak strain increases. However, the strain growth factors of Shell 1 subjected to different first peak strains vary in a narrow range between 3.3 and 4.4, as shown in Fig.10.

As shown in Section 3.1.2, the response of Shell 1 is stable when its first peak strain (0.0005) is small. Mathieu diagram of Shell 1 with first peak strain of 0.0005 is drawn in Fig.11, which shows that all the vibration modes are stable. Therefore, the dynamic unstable response may not happen in a spherical shell with small first peak strain, indicating that strain growth may be avoided by reducing the first peak strain.

3.2.3 The radius-to-thickness ratio

The effect of the radius-to-thickness ratio on the occurrence of strain growth is examined by comparing the responses between Shell 1 and Shell 2 with the same first peak strain. In the dynamic response history of Shell 2, whose dimensions and material parameters are listed in Table 3, the nonlinear modal coupling response is not observed when the first peak strain is 0.005. According to McIvor and Sonstegard(1966), Mathieu diagram of Shell 2 with a first peak strain of 0.005 is drawn in Fig.12, which shows that all the vibration modes are stable. With the same first peak strain, strain growth happens in Shell 1 but not in Shell 2, indicating that the nonlinear modal coupling in spherical shells is controlled by choosing the proper radius-to-thickness ratio. Actually, McIvor and Sonstegard(1966) observed that the smaller the radius-to-thickness ratio is, the more unstable composite modes are.

Predictions for the the occurrence of the dynamic unstable vibration in Figs.8, 11 and 12 based on McIvor and Sonstegard(1966)'s method on the axisymmetric response of spherical shells demonstrate good agreement with the simulation results obtained by LS-DYNA on the nonaxisymmetric response of spherical shells. Therefore, the numerical results support the Postulate-1 in Section 3.1.3.

3.3 Design considerations for the control of strain growth in containment vessels

It has been shown that the first peak strain and radius-to-thickness ratio are two dominant factors influencing strain growth caused by nonlinear modal coupling. Strain growth due to nonlinear modal coupling may be avoided by reducing the first peak strain or choosing a proper radius-to-thickness ratio. The occurrence of strain growth is sensitive to the radius-to-thickness ratio, and thus, the structural dimensions should be carefully selected.

Combining Eq.(10) and Hooke's law $\sigma = E\varepsilon/(1-\nu)$, we obtain (McIvor and Sonstegard 1966)

$$\frac{v_0}{c} = \frac{\sigma_0}{E}\omega_0(1-\nu), \tag{14}$$

where σ_0 is the yield stress. According to McIvor and Sonstegard(1966), the maximum value of σ_0/E in practical use is 0.005. Therefore, for Shell 1 with $\nu = 0.3$, $\omega_0 = 1.612$ and the maximum value of v_0/c is 0.005646.

In order to study the effect of the radius-to-thickness ratio, the dynamic instabilities caused by nonlinear modal coupling in 81 spherical shells are examined. The radius-to-thickness ratios range from 20 to 100, in which the increment is 1. The values of v_0/c applied on shells are 0.001, 0.002, 0.003, 0.004, 0.005 and 0.005646, respectively. The value of (Ω_n, μ_n) for the 81 shells with different

values of v_0/c are calculated according to Eq.(4). Results of the dynamic instability analysis for 81 spherical shells with different radius-to-thickness ratios and values of v_0/c are presented in Fig.13, in which the stable and unstable regions are marked. As only six values of v_0/c are chosen, the gap between the stable and unstable regions are marked as unknown region. It can be observed that the thicker spherical shells, especially those with the radius-to-thickness ratio ranging from 20 to 25, have less chance to show strain growth even when v_0/c is very large (i.e. 0.005646 in the present simulation).

Probability analyses on the dynamic instability of 81 shells are carried out, as presented in Table 4 and Fig.14. It shows that the overall possibility of unstable vibration in thicker shells is smaller, and the possibility of unstable vibration in shells with lower first peak strain is smaller. However, it is also interesting to observe that when values of v_0/c are 0.005 and 0.005646, the percentages of instability of shells with a/h in the range of 38-46 are higher than those of shells with a/h in the range of 47-55, which indicates that the occurrence of dynamic unstable vibration is also a parameter sensitive problem. The considerations for the control of strain growth discussed in this section may provide engineering guidelines for the design of spherical containment vessels.

4. Conclusions

1. The strain growth observed in nonaxisymmetric response of a complete spherical shell subjected to uniformly-distributed internal blast loading can be explained by the nonlinear coupling between the radial breathing mode and the composite modes.
2. First peak strain and the radius-to-thickness ratio are the dominant factors influencing strain growth in spherical shells caused by nonlinear modal coupling. Strain growth may be avoided by reducing the first peak strain or choosing proper radius-to-thickness ratios.
3. The analytical method on the axisymmetric responses of spherical shells in McIvor and Sonstegard(1966) may be employed to predict the occurrence of the dynamic unstable vibration in the nonaxisymmetric responses of spherical shells.
4. To design a spherical shell with smaller radius-to-thickness ratio may avoid the occurrence of strain growth. Dynamic instability analysis results in Figs.13 and 14 may be employed to guide the design of spherical containment vessels.

Acknowledgements: The first author acknowledges the financial support from ORS award, the scholarship from the School of Mechanical, Aerospace and Civil Engineering at The University of Manchester and from Henry Lester Trust. The third author acknowledges the support from the National Science Foundation of China (NSFC) under contract no.50675195.

References

Abakumov AI, Egunov VV, Ivanov AG, Uchaev AA, Tsypkin VI, Shitov AT(1984), Calculation and experiments on the deformation of explosion-chamber shells, Zhurnal Prikladnoi Mekhaniki i Tekhnicheskoi Fiziki, (3), 127-130.

ANSYS, Inc.(2004), ANSYS Structural Analysis Guide.

Baker WE(1960), The elastic-plastic response of thin spherical shells to internal blast loading, ASME J. Appl. Mech., 27, 139-144.

Baker WE(1961), Axisymmetric Modes of Vibration of Thin Spherical Shell, J. Acoust. Soc. Am., 33(12), pp. 1749–1758.

Belov AI, Klapovskii VE, Kornilo VA, Mineev VN, Shiyan VS(1984), Dynamics of a spherical shell under a nonsymmetric internal pulse loading, Fiz Goreniya Vzryva, 20(3), 71-74.

Buzukov AA(1976), Characteristics of the behavior of the walls of explosion chambers under the action of pulsed loading, Fiz Goreniya Vzryva, 12(4), 605-610.

Buzukov AA(1980), Forces produced by an explosion in an air-filled explosion chamber, Fiz Goreniya Vzryva, 16(5), 87-93.

Dong Q, Li QM and Zheng JY(2008), Investigation on the mechanisms of strain growth in cylindrical containment vessels subjected to internal blast loading, Proceedings of 2008 ASME Pressure Vessels and Piping Conference, Chicago, ASME Press.

Duffey TA, Romero C(2003), Strain growth in spherical explosive chambers subjected to internal blast loading, Int. J. Impact Eng, 28, 967-983.

Duffey TA, Pepin JE, Robertson AN, Steinzig ML and Coleman K(2007), Vibrations of complete spherical shells with imperfections, J. Vibration and Acoustics, 129, 363-370.

Kalnins A(1964), Effect of Bending on Vibrations of Spherical Shells, J. Acoust. Soc. Am., 36(1), pp. 74–81.

Karpp RR, Duffey TA, Neal TR(1983), Response of containment vessels to explosive blast loading, ASME. J. Pressure Vessel Tech., 105, 23-27.

Kornev VM, Adishchev VV, Mitrofanov AN, Grekhov VA(1979), Experimental investigation and analysis of the vibrations of the shell of an explosion chamber, Fiz Goreniya Vzryva, 15(6), 155-157.

Li QM, Dong Q, Zheng JY(2008), Strain growth of the in-plane response in an elastic cylindrical shell, Int. J. Impact Engng, 35(10), 1130-1153.

Livermore Software Technology Corporation(1998), LS-DYNA theoretical manual.

Livermore Software Technology Corporation(2003), LS-DYNA keyword user's manual (Version 970).

Mal'tsev VA, Konon YA, Adishchev VV, Kornev VM(1984), Experimental study and analysis of the vibrations of an impulsively loaded thin-walled spherical shell, Fiz Goreniya Vzryva, 20(2),

97-102.

McIvor IK and Sonstegard DA(1966), Axisymmetric response of a closed spherical shell to nearly uniform radial impulse, J. Acoust. Soc. Am., 40(6), pp. 1540-1547.

McLachlan NW(1947), Theory and application of Mathieu functions, Clarendon Press, Oxford.

Nayfeh AH and Arafat HN(2006), Axisymmetric vibrations of closed spherical shells: Equations of motion and bifurcation analysis, Struct. Control Health Monit., 13, pp. 388-416.

Nickell R. E., Romero C(2003), Containing explosions, Mechanical Engineering, 125(9), 62-72.

Niordson FI(1984), Free vibrations of thin elastic spherical shells, Int. J. Solids Struct., 20, pp. 667–687.

Niordson FI(1988), The spectrum of free vibrations of a thin elastic spherical shell, Int. J. Solids Struct., 24, 947-961.

Shah AH, Ramkrishnan CV, Datta SK (1969), Three-dimensional and shell-theory analysis of elastic waves in a hollow sphere, J. Appl. Mech., 36, 431-439.

Silbiger A(1960), Free and forced vibrations of a spherical shell, CAA, Inc. Report U-106-48.

Silbiger A(1965), Nonaxisymmetric modes of vibration of thin spherical shells, J. Acoust. Soc. Am., 38, pp. 367–368.

Wilkinson JP(1965), Natural Frequencies of Closed Spherical Shells, J. Acoust. Soc. Am., 38(2), pp. 367–368.

Zhdan SA(1981), Dynamic load acting on the wall of an explosion chamber, Fiz Goreniya Vzryva, 17(2), 142-146.

Zheng JY, Deng GD, Chen YJ, Sun GY, Hu YL, Zhao LM, Li QM(2006), Experimental investigation of discrete multilayered vessels under internal explosion, Combustion, Explosion, and Shock Waves, 42(5): 616-622.

Zhu WH, Xue HL, Zhou GQ, Schleyer GK(1997), Dynamic response of cylindrical explosive chambers to internal blast loading produced by a concentrated charge, Int. J. Impact Eng, 19(9-10), 831-845.

Table list

Figure list

Fig.1. Axisymmetric and nonaxisymmetric mode shapes for n=5, m=0 (axisymmetric mode) and m=1, 2, … 5 (non-axisymmetric modes) in lower branch (Duffey et al. 2007).

Fig.2. (a) Radial displacement-time history of the response of complete spherical Shell 1 subjected to impulsive loading (first peak strain is 0.0005), (b) The frequency spectrum of the curve in Fig.2 (a).

Fig.3. Natural frequencies of vibration modes in Shell 1 using Eq.(2).

Fig.4. (a) Radial displacement-time history of the response of complete spherical Shell 1 subjected to impulsive loading (first peak strain is 0.005), (b) The frequency spectrum of the curve in Fig.4(a).

Fig.5. Circumferential displacement-time history of the response of complete spherical Shell 1 subjected to impulsive loading (first peak strain is 0.005).

Fig.6. Longitudinal displacement-time history of the response of complete spherical Shell 1 subjected to impulsive loading (first peak strain is 0.005).

Fig.7. The deformed shapes of spherical Shell 1 from different view directions (first peak strain is 0.005) (The displacement has been multiplied by 10).

Fig.8. Mathieu diagram of Shell 1 with a first peak strain of 0.005.

Fig.9. Relationships between t_p/T_0 and the first peak strain.

Fig.10. Relationships between K_p and the first peak strain.

Fig.11. Mathieu diagram of Shell 1 with a first peak strain of 0.0005.

Fig.12. Mathieu diagram of Shell 2 with a first peak strain of 0.005.

Fig.13. Results of the dynamic instability analysis for 81 spherical shells with various radius-to-thickness ratios and v_0/c values.

Fig.14. Probability analyses on 81 shells with the various radius-to-thickness ratios and v_0/c values.

Table 1 Dimensions and material parameters of Shell 1

Mean radius a	Thickness h	Young's modulus E	Poisson's ratio ν	Density ρ
200 mm	2 mm	210 GPa	0.3	7830 kg/m^3

Table 2 Responses of complete spherical Shell 1 subjected to impulsive loadings

First peak radial displacement	First peak strain	Maximum radial displacement	Strain growth factor K_p	Strain growth time t_P	t_P / T_0
0.079 cm	0.0040	0.267 cm	3.380	5.44 ms	37.9
0.089 cm	0.0045	0.351 cm	3.944	3.17 ms	22.1
0.099 cm	0.0050	0.375 cm	3.788	2.29 ms	16.0
0.109 cm	0.0055	0.479 cm	4.394	2.02 ms	14.1
0.119 cm	0.0060	0.475 cm	3.992	1.72 ms	12.0

Table 3 Dimensions and material parameters of Shell 2

Mean radius a	Thickness h	Young's modulus E	Poisson's ratio ν	Density ρ
41 mm	2 mm	210 GPa	0.3	7830 kg/m^3

Table 4 Numbers of unstable shells with different values of v_0/c

a/h v_0/c	20-28	29-37	38-46	47-55	56-64	65-73	74-82	83-91	92-100	20-100
0.001	0	0	0	0	1	1	1	1	2	6
0.002	0	0	1	1	1	2	4	4	5	18
0.003	0	1	3	1	3	4	5	6	6	29
0.004	1	1	3	3	4	6	7	7	9	41
0.005	1	2	5	3	5	7	9	9	9	50
0.005646	1	2	5	4	6	9	9	9	9	54

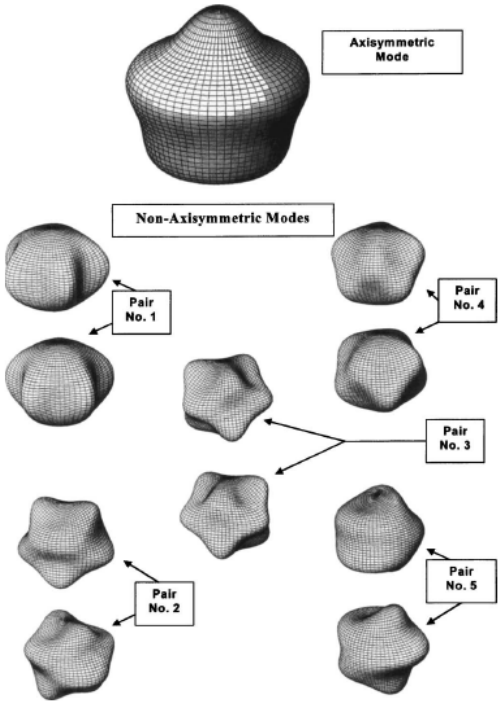

Fig.1. Axisymmetric and nonaxisymmetric mode shapes for n=5, m=0 (axisymmetric mode) and m=1, 2, … 5 (non-axisymmetric modes) in lower branch (Duffey et al. 2007).

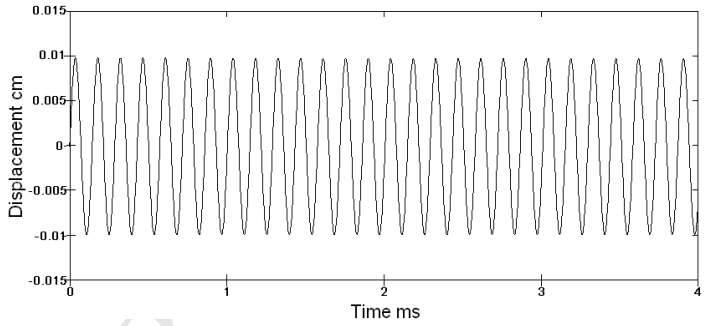

(a)

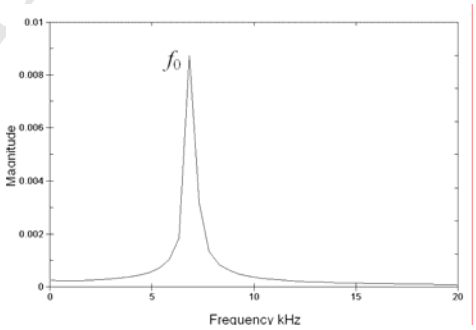

(b)

Fig.2. (a) Radial displacement-time history of the response of complete spherical Shell 1 subjected to impulsive loading (first peak strain is 0.0005), (b) The frequency spectrum of the curve in Fig.2 (a).

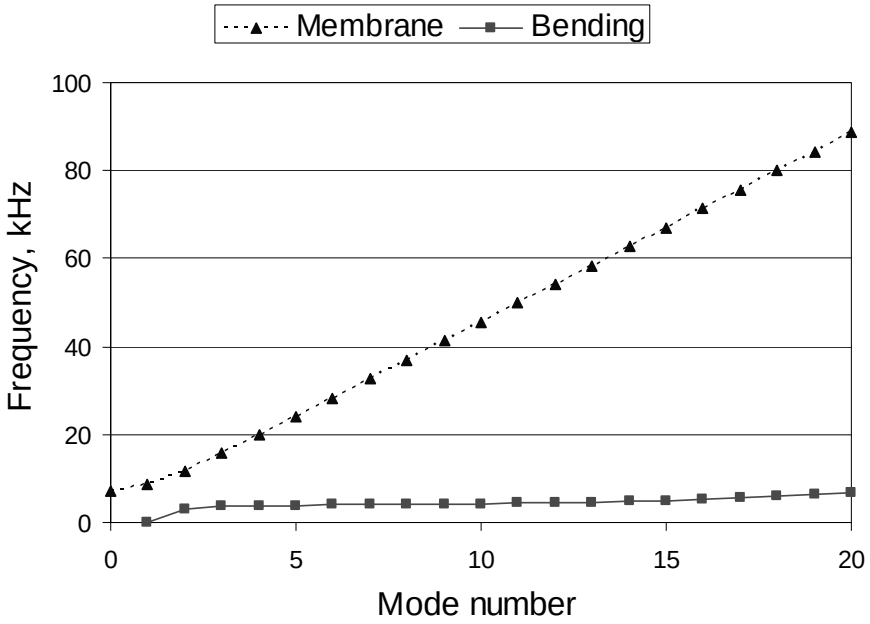

Fig.3. Natural frequencies of vibration modes in Shell 1 using Eq.(2).

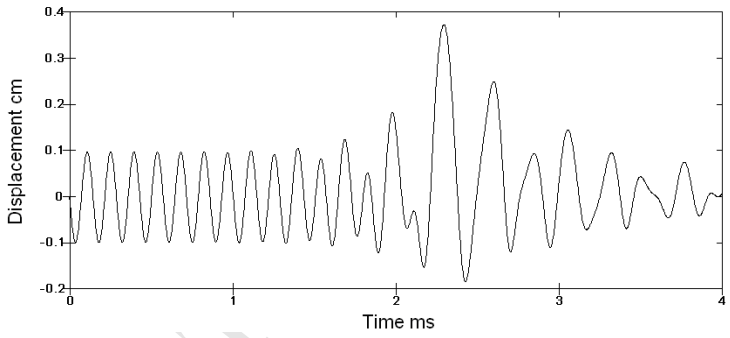

(a)

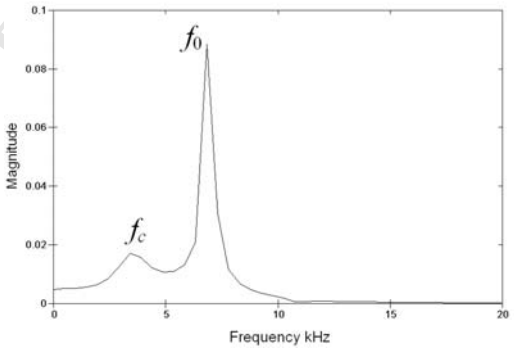

(b)

Fig.4. (a) Radial displacement-time history of the response of complete spherical Shell 1 subjected to impulsive loading (first peak strain is 0.005), (b) The frequency spectrum of the curve in Fig.4(a).

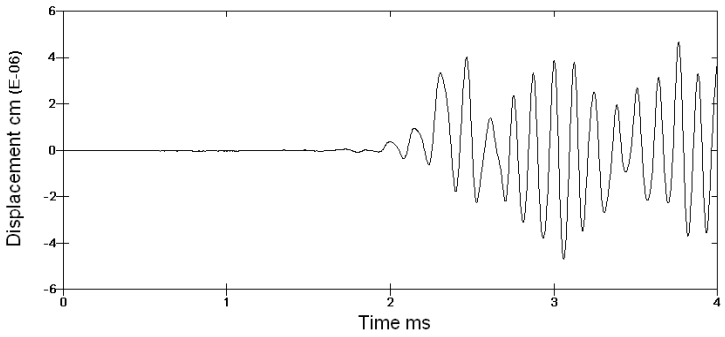

Fig.5. Circumferential displacement-time history of the response of complete spherical Shell 1 subjected to impulsive loading (first peak strain is 0.005).

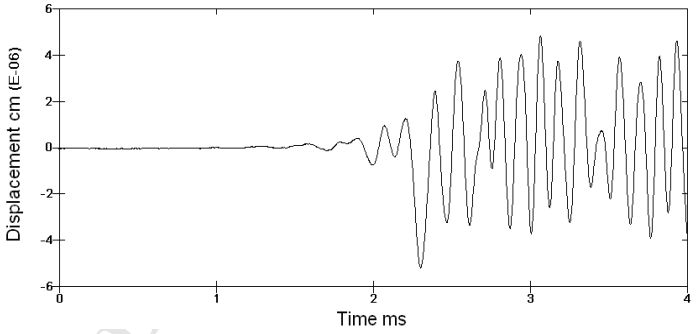

Fig.6. Longitudinal displacement-time history of the response of complete spherical Shell 1 subjected to impulsive loading (first peak strain is 0.005).

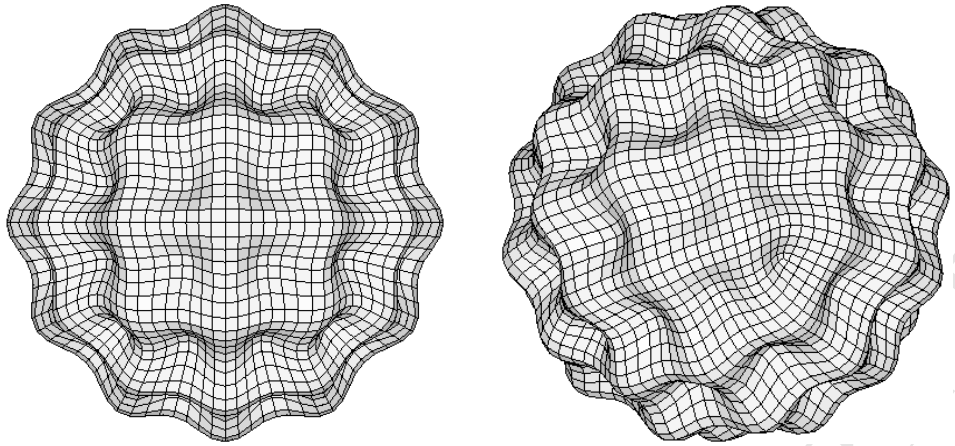

(a) (b)

Fig.7. The deformed shapes of spherical Shell 1 from different view directions (first peak strain is 0.005) (The displacement has been multiplied by 10).

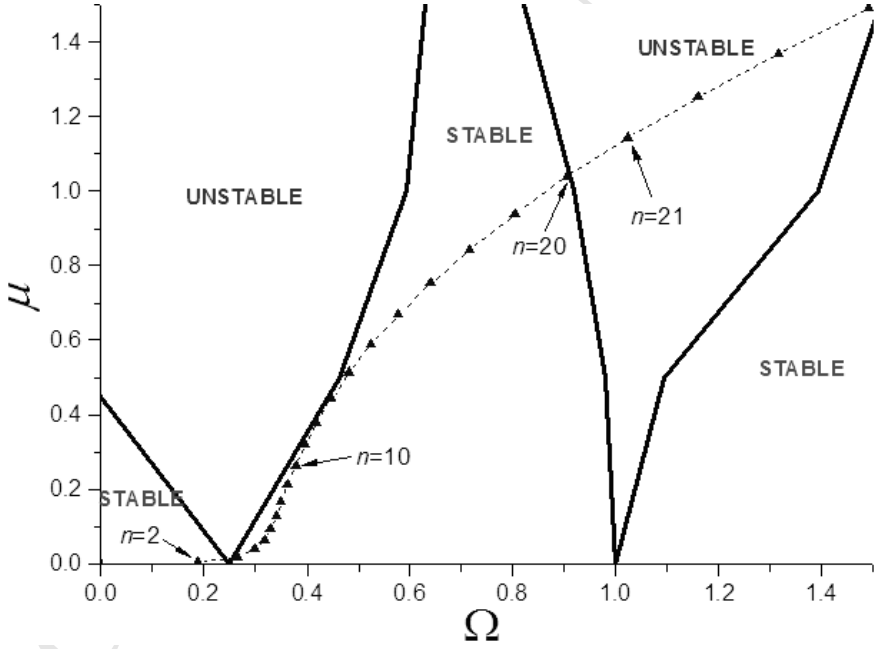

Fig.8. Mathieu diagram of Shell 1 with a first peak strain 0.005.

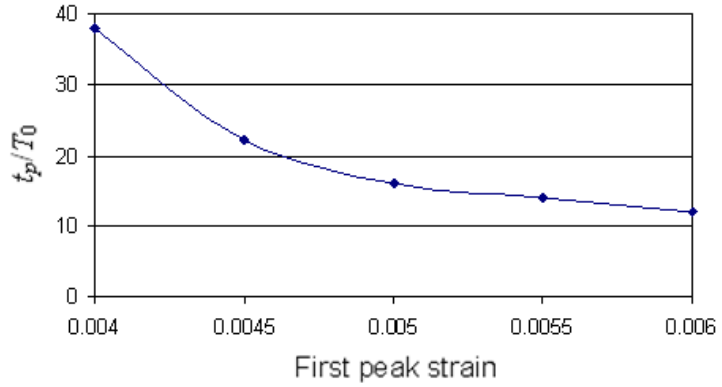

Fig.9. Relationships between t_p/T_0 and the first peak strain.

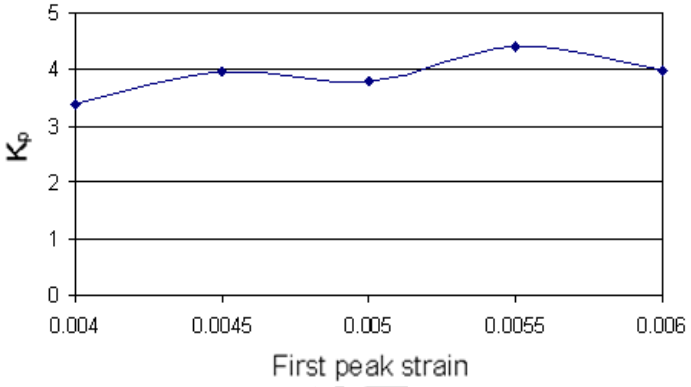

Fig.10. Relationships between K_p and the first peak strain.

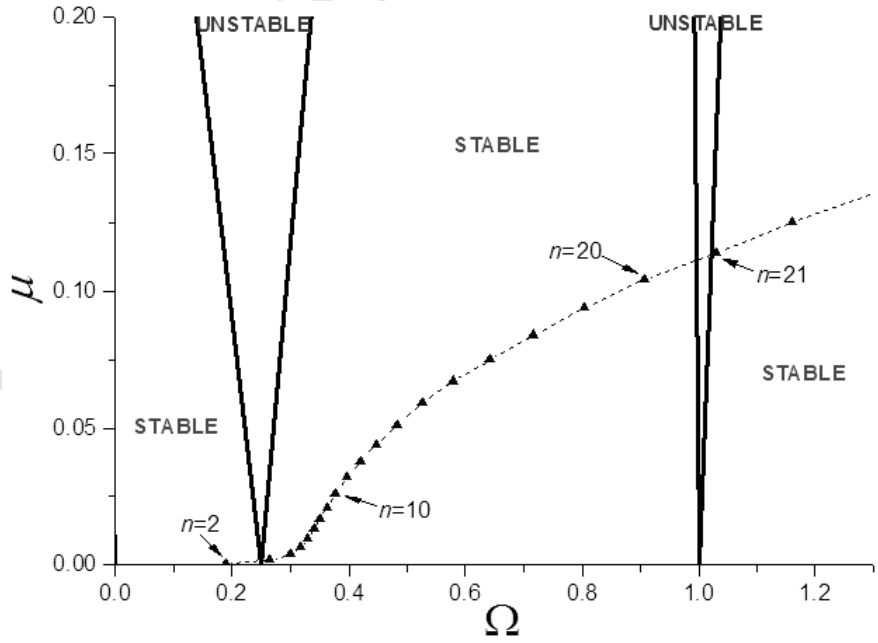

Fig.11. Mathieu diagram of Shell 1 with a first peak strain 0.0005.

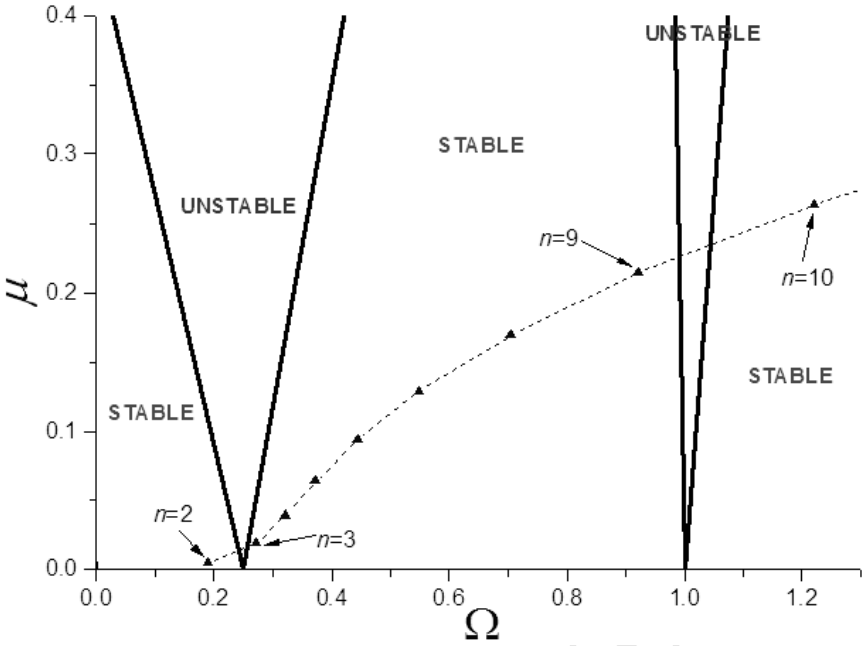

Fig.12. Mathieu diagram of Shell 2 with a first peak strain 0.005.

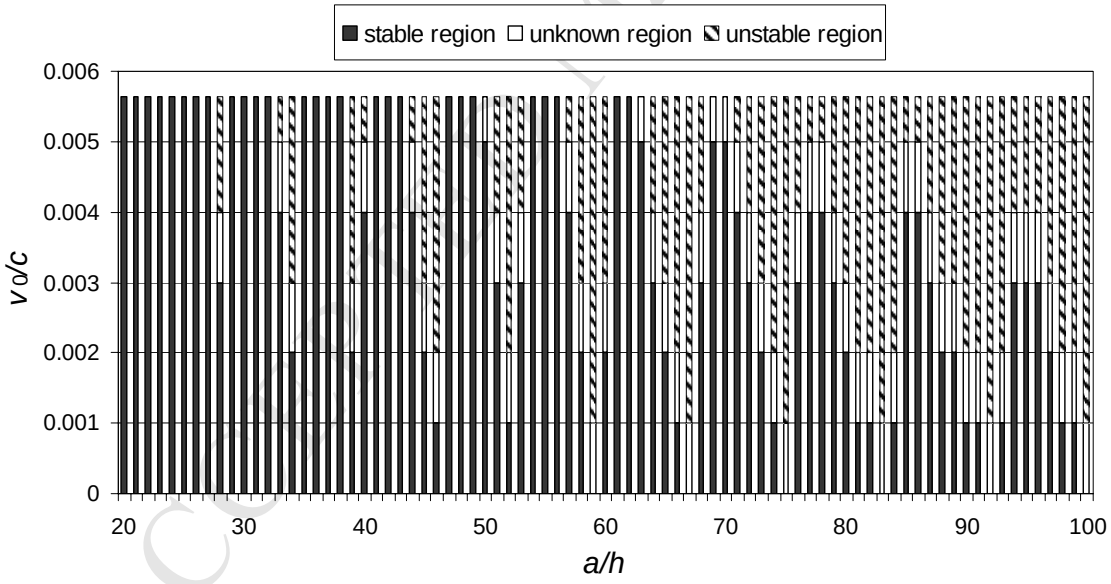

Fig.13. Results of the dynamic instability analysis for 81 spherical shells with various radius-to-thickness ratios and v_0/c values.

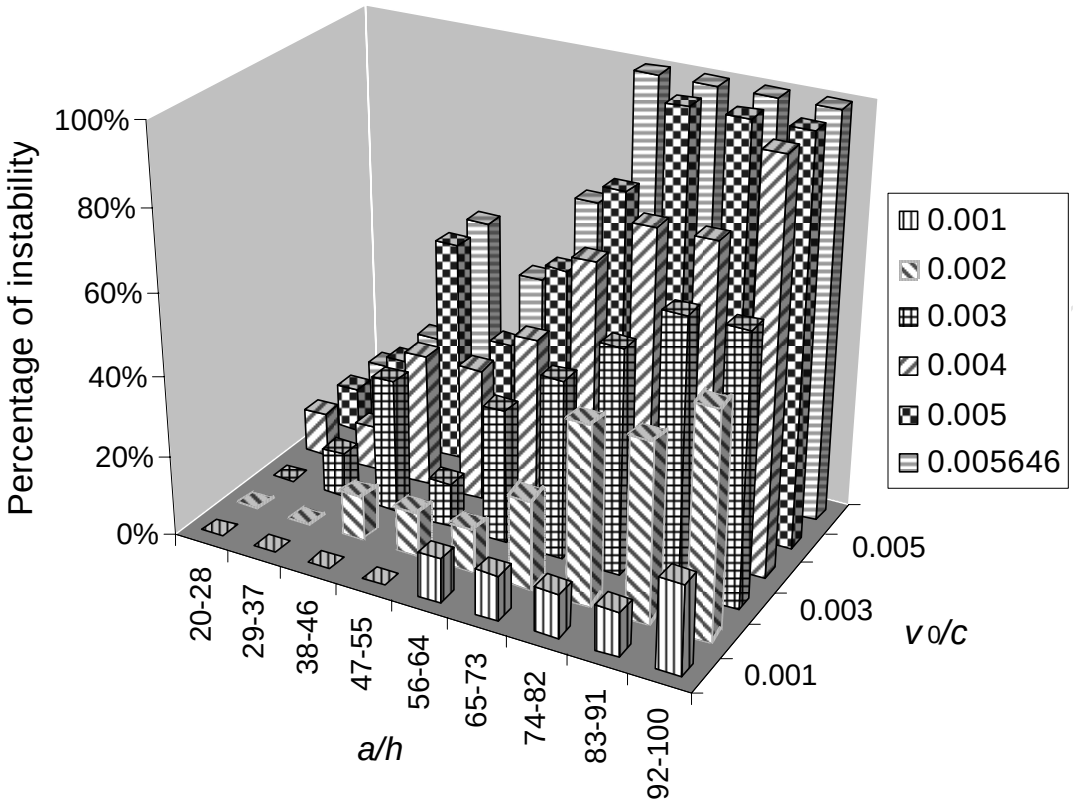

Fig.14. Probability analyses on 81 shells with the various radius-to-thickness ratios and v_0/c values